Second-Harmonic Generation from Magnetic Metamaterials

Matthias W. Klein, *et al.*

Science **313**, 502 (2006);
DOI: 10.1126/science.1129198

conditions, the simulated traces are virtually free of adjustable parameters as $C \geq 4C_\mu \gg C_q$.

It is important to note that in a real system, the weak transmission regime is accompanied by Coulomb blockade effects that are not taken into account in the above model. In the weak transmission regime and $T = 0$, using an elastic cotunneling approach (*23*, *24*), we have checked that there is no qualitative change except for the energy scale that now includes the charging energy so that Δ is replaced by $\Delta + e^2/C = e^2/C_\mu$. At large transmission, the problem is nonperturbative in tunnel coupling and highly nontrivial. Calculations of the thermodynamic capacitance exist [(*25*, *26*), and (*27*) plus references therein], but at present, no comprehensive model is available that would include both charge-relaxation resistance and quantum capacitance for finite temperature and/or large transmission.

Calibration of our admittance measurements is a crucial step toward extracting the absolute value of the constant charge-relaxation resistance. As at GHz frequencies, direct calibration of the whole detection chain is hardly better than 3 dB, we shall use here an indirect, but absolute, method, often used in Coulomb blockade spectroscopy, that relies on the comparison between the gate voltage width of a thermally broadened Coulomb peak ($\propto k_BT$) and the Coulomb peak spacing ($\propto e^2/C_\mu$). From this, an absolute value of C_μ can be obtained. The real part of the admittance of sample E3 is shown as a function of the dc voltage V_{dc} at the counter-electrode, for a given low transmission (Fig. 3A). A series of peaks with periodicity $\Delta V_{dc} = 370$ μV are observed, with the peaks accurately fitted by Eq. 7. Their width, proportional to the electronic temperature T_{el}, is plotted versus the refrigerator temperature T (see Fig. 3C). When corrected for apparent electron heating arising from gaussian environmental charge noise, and if we assume $T_{el} = \sqrt{(T^2 + T_0^2)}$, the energy calibration of the gate voltage yields C_μ and the amplitude $1/C_\mu\omega$ of the conductance plateau in Fig. 2. A similar analysis is done in Fig. 3, B and D, for sample E1 using V_G to control the dot potential. Here, peaks are distorted because of a transmission-dependent background and show a larger periodicity $\Delta V_G = 2$ mV, which reflects the weaker electrostatic coupling to the 2DEG.

Finally, after numerical inversion of the conductance data, we can separate the complex impedance into the contributions of the capacitance, $1/C_\mu\omega$, and the relaxation resistance R_q. The results in Fig. 4 demonstrate deviations from standard Kirschhoff's laws: The charge-relaxation resistance R_q remains constant in the regime where the quantum capacitance exhibits strong transmission-dependent oscillations; this constant value equals, within experimental uncertainty, half the resistance quantum as prescribed by theory (*9*, *10*). In the weak transmission regime, the Landauer formula is recovered because of thermal broadening, and R_q diverges as it does in the dc regime. Furthermore, additional measurements at 4 *K* prove that the classical behavior is indeed recovered in the whole transmission range whenever $k_BT \gg e^2/C_\mu$.

In conclusion, we have experimentally shown that the series association of a quantum capacitor and a model quantum resistor leads to a violation of the dynamical Kirchhoff's law of impedance addition. In the fully coherent regime, the quantum resistor is no longer given by the Landauer formula but by the half-quantized charge-relaxation resistance predicted in refs. (*9*, *10*).

References and Notes

1. R. Landauer, *IBM J. Res. Dev.* **1**, 233 (1957).
2. R. Landauer, *Phil. Mag.* **21**, 863 (1970).
3. P. W. Anderson, *Phys. Rev. B* **23**, 4828 (1981).
4. M. Büttiker, Y. Imry, R. Landauer, S. Pinhas, *Phys. Rev. B* **31**, 6207 (1985).
5. B. Gao, A. Komnik, R. Egger, D. C. Glattli, A. Bachtold, *Phys. Rev. Lett.* **92**, 216804 (2004).
6. See for a review, S. Datta, *Electronic Transport in Mesoscopic Systems* (Cambridge Univ. Press, Cambridge, 1997).
7. See for a review, Y. Imry, *Introduction to Mesoscopic Physics* (Oxford Univ. Press, Oxford, 1997).
8. M. Büttiker, *Phys. Rev. Lett.* **57**, 1761 (1986).
9. M. Büttiker, A. Prêtre, H. Thomas, *Phys. Rev. Lett.* **70**, 4114 (1993).
10. A. Prêtre, H. Thomas, M. Büttiker, *Phys. Rev. B* **54**, 8130 (1996).
11. S. Pilgram, M. Büttiker, *Phys. Rev. Lett.* **89**, 200401 (2002).
12. A. A. Clerk, S. M. Girvin, A. D. Stone, *Phys. Rev. B* **67**, 165324 (2003).
13. M. Büttiker, H. Thomas, A. Prêtre, *Phys. Lett. A* **180**, 364 (1993).
14. Ya. M. Blanter, M. Büttiker, *Phys. Rep.* **336**, 1 (2000).
15. F. W. J. Hekking, J. P. Pekola, *Phys. Rev. Lett.* **96**, 056603 (2006).
16. G. Seelig, S. Pilgram, A. N. Jordan, M. Büttiker, *Phys. Rev. B* **68**, 161310 (2003).
17. P. J. Burke, *IEEE T. Nanotechnol.* **2** (1), 55 (2003).
18. R. C. Ashoori *et al.*, *Phys. Rev. Lett.* **68**, 3088 (1992).
19. R. C. Ashoori *et al.*, *Phys. Rev. Lett.* **71**, 613 (1992).
20. Materials and methods are available as supporting material on *Science* Online.
21. J. Gabelli, thesis, Université Pierre et Marie Curie, Paris, 2006; online access at (http://tel.ccsd.cnrs.fr/tel00011619).
22. M. Büttiker, *Phys. Rev. B* **41**, 7906 (1990).
23. D. V. Averin, Y. Nazarov, in *Single Charge Tunneling* (NATO ASI ser. B, vol. 294, Plenum, New York, 1992), chap. 6.
24. D. C. Glattli, *Physica B* **189**, 88 (1993).
25. K. A. Matveev, *Phys. Rev. B* **51**, 1743 (1995).
26. L. I. Glazman, I. L. Aleiner, *Phys. Rev. B* **57**, 9608 (1998).
27. P. W. Brouwer, A. Lamacraft, K. Flensberg, *Phys. Rev. B* **72**, 075316 (2005).

28. The Laboratoire Pierre Aigrain is the CNRS-ENS UMR8551 associated with universities Paris 6 and Paris 7. The research has been supported by AC-Nanoscience, SESAME grants, and ANR-05-NANO-028.

Supporting Online Material

www.sciencemag.org/cgi/content/full/1126940/DC1
Materials and Methods

2 March 2006; accepted 26 June 2006
Published online 13 July 2006;
10.1126/science.1126940
Include this information when citing this paper.

Second-Harmonic Generation from Magnetic Metamaterials

Matthias W. Klein,[1,2] Christian Enkrich,[1,2] Martin Wegener,[1,2,3] Stefan Linden[1,2,3]*

We observe second-harmonic generation from metamaterials composed of split-ring resonators excited at 1.5-micrometer wavelength. Much larger signals are detected when magnetic-dipole resonances are excited, as compared with purely electric-dipole resonances. The experiments are consistent with calculations based on the magnetic component of the Lorentz force exerted on metal electrons—an intrinsic second-harmonic generation mechanism that plays no role in natural materials. This unusual mechanism becomes relevant in our work as a result of the enhancement and the orientation of the local magnetic fields associated with the magnetic-dipole resonances of the split-ring resonators.

The concept of metamaterials has changed the spirit of optics and photonics. Researchers no longer just study the rich variety of materials provided by nature but have rather become creative designers who tailor optical properties at will, leading to qualitatively new and unprecedented behavior (*1*–*11*). The key is the nanofabrication of metallic subwavelength-scale functional building blocks, photonic atoms, which are densely packed into an effective material. To a large extent, this emerging field has been stimulated by the 1999 theoretical work of John Pendry's group (*1*), which made two distinct predictions: (i) They proposed split-ring resonators as photonic atoms that could lead to magnetism at optical frequencies—a prerequisite for negative-index metamaterials. (ii) Furthermore, they predicted that enhanced and novel nonlinear-optical properties could arise from such metamaterials. Although aspect (i) has attracted substantial attention from both experiment (*3*–*7*, *12*, *13*) and theory (*14*–*16*) in recent years, aspect (ii) has not, to the best of our knowledge. Experiments have not been reported, nor has a complete consistent microscopic theory of the nonlinear optics of metamaterials been evaluated. This lack of re-

[1]Institut für Angewandte Physik, Universität Karlsruhe (TH), Wolfgang-Gaede-Straße 1, D-76131 Karlsruhe, Germany. [2]DFG-Center for Functional Nanostructures (CFN), Universität Karlsruhe (TH), D-76128 Karlsruhe, Germany. [3]Institut für Nanotechnologie, Forschungszentrum Karlsruhe in der Helmholtz-Gemeinschaft, D-76021 Karlsruhe, Germany.

*To whom correspondence should be addressed. E-mail: stefan.linden@physik.uni-karlsruhe.de

search is contrasted by the potential of metamaterials for giant nonlinear-optical response through local-field enhancements (*1*, *15*) and/or novel mechanisms. This avenue could, for example, lead to ultracompact frequency-doubling devices. Ultimately, parametric nonlinear-optical processes (*17*) in metamaterials might possibly even be used as a gain mechanism, compensating the metamaterial absorption losses in, for example, "perfect lenses" (*2*, *18*). Here, we make steps in direction (ii) and study the lowest-order nonlinear-optical process, that is, second-harmonic generation (SHG). We directly compare our experimental findings on arrays of gold split-ring resonators (SRRs) with the results of a simple theory based on the magnetic component of the Lorentz force on metal electrons in the SRRs—an intrinsic second-harmonic generation mechanism that plays no role in natural materials.

In fact, in usual nonlinear optics, the magnetic-field component of the electromagnetic light wave hardly plays any immediate role at all. Rather, electric dipoles are excited by the electric-field component of the light only. There are, however, some exotic cases of nonlinear optics governed by the magnetic component that we would like to recall before describing our own work. Generally, the magnetic field $\boldsymbol{B}$ enters by means of the magnetic component of the Lorentz force, $\boldsymbol{F} = q(\boldsymbol{E} + \boldsymbol{v} \times \boldsymbol{B})$, where q and $\boldsymbol{v}$ are the electron charge and velocity, respectively. Although the modulus of the $q(\boldsymbol{v} \times \boldsymbol{B})$ term becomes comparable in strength to the electric component of the Lorentz force $q\boldsymbol{E}$ only for relativistic velocities $\boldsymbol{v}$, it has measurable consequences for optical frequencies at much smaller velocities. For example, it can lead to the photon-drag effect (*19*), a drift velocity of free crystal electrons that is proportional to the intensity of light and directed along the wave vector of light. This effect is employed in commercially available infrared photon-drag p-type germanium photodetectors and can be interpreted as the dynamic Hall effect (*20*). On the same order of perturbation theory in the incident fields, one also gets an oscillatory electron motion at twice the exciting light frequency (*21*). The polarization of the resulting SHG is again directed along the incident wave vector of light. Such SHG has been observed for free vacuum electrons and is called nonlinear Thomson scattering (*19*, *21*) or Larmor radiation. All these nonlinear contributions point in the direction of the incident wave vector of light $\boldsymbol{K} \sim (\boldsymbol{v} \times \boldsymbol{B}) \sim (\boldsymbol{E} \times \boldsymbol{B})$; they are longitudinal components, which cannot propagate in the forward direction. In contrast, a significant component of the local magnetic field pointing along the direction of the incident wave vector of light, as in some of our SRR structures below, could clearly lead to a transverse component of SHG. A transverse component, in contrast to a longitudinal component, can efficiently be radiated into the far-field forward direction. For the symmetry of the structures to be discussed below, this transverse SHG would be polarized orthogonal to the electric-field component of the incident light, hence perpendicular to the incident linear polarization.

The metamaterials under investigation are planar arrays of SRRs. Each SRR can be viewed as a small *LC*-oscillator circuit. The open ends of a nonmagnetic gold wire form the capacitance C; the wire itself is a fraction of one winding of a magnetic coil with inductance L (see insets in Fig. 1). The corresponding magnetic dipole moment is oriented perpendicular to the plane of the SRR. Details of design, fabrication and linear-optical characterization of the magnetic metamaterials used here have been described elsewhere (*5*, *6*). Briefly, 100-μm by 100-μm two-dimensional arrays of gold split rings with variable lateral size l and thickness t = 25 nm, on a square lattice with variable lattice constant a, are fabricated on glass substrates coated with a 5-nm thin film of indium-tin-oxide (ITO) with standard electron-beam lithography. The eigenfrequency of our *LC* circuit scales inversely with SRR size, provided the eigenfrequency is much smaller than the bulk metal plasma frequency. For normal incidence and horizontal polarization, the electric field of the light can couple to the capacitance (*5*, *6*), inducing a circulating current in the coil, leading to an oscillatory magnetic dipole moment perpendicular to the SRR plane. This resonant circulating current leads to a resonant enhancement of the local magnetic fields. For vertical incident polarization, neither the electric nor the magnetic component of the light can couple to the *LC* resonance. For both linear polarizations one can, however, excite the SRR Mie resonance, which is located at frequencies higher than that of the *LC* resonance. When exciting the Mie resonance with horizontal incident polarization, the current in the SRR bottom arm is accompanied by currents in the two vertical SRR arms. The latter two oscillate 180 degrees out of phase; hence, one gets a nonzero magnetic-dipole moment (*6*). In contrast, for vertical incident polarization, the response of the Mie resonance is purely electric. Corresponding measured transmittance spectra of the samples investigated here are shown in Fig. 1. The various observed transmittance dips correspond to the resonances discussed above. These two samples as well as others are located on the same glass substrate and have been fabricated in one run.

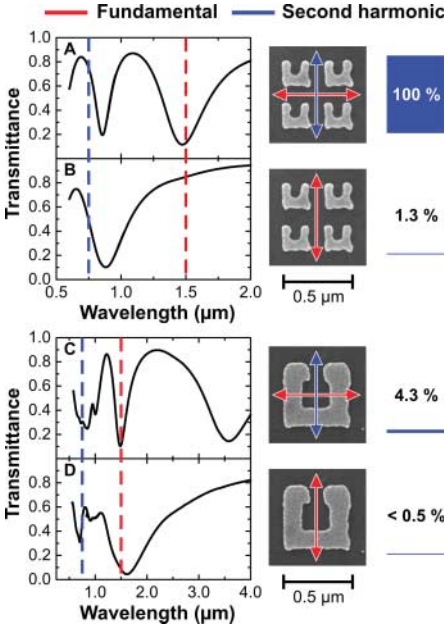

Fig. 1. Summary of measured linear-optical spectra (black solid curves), shown for two relevant magnetic metamaterial samples located on the same substrate. The polarization of the incident light is indicated by the red arrows in the electron micrographs of the corresponding structures. The wavelengths of the exciting light (red) and that of the SHG (blue) are indicated by dashed lines. (**A**) and (**B**) correspond to an array with small SRRs (l = 220 nm, a = 305 nm), (**C**) and (**D**) to an array with large SRRs (l = 480 nm, a = 630 nm). The blue bars highlight the corresponding measured SHG signal strengths, normalized to 100% for the strongest SHG signal obtained from the fundamental magnetic (or *LC*) resonance. The detection noise is about 0.2%. The approximate polarization of the SHG emission is indicated by the blue arrows (see also Fig. 2B).

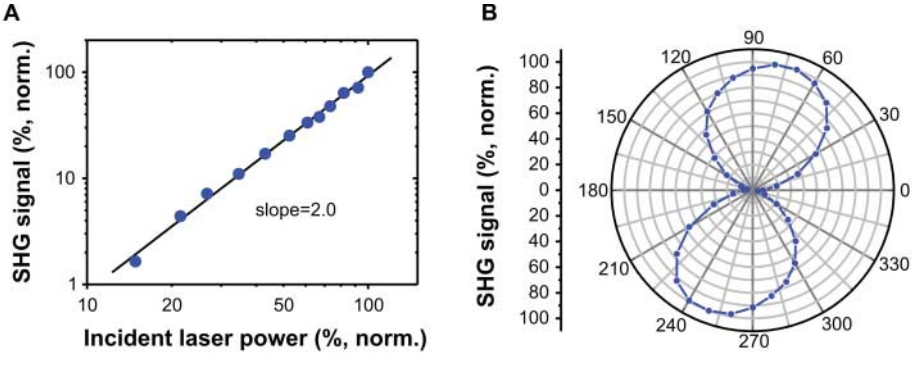

Fig. 2. (**A**) Normalized SHG signal strength versus normalized incident laser power on a log-log scale (for the fundamental magnetic resonance in Fig. 1A). The straight line has a slope of two, as expected for SHG. (**B**) Measured polarization of the SHG emission represented as a polar diagram, oriented as the electron micrograph in Fig. 1A.

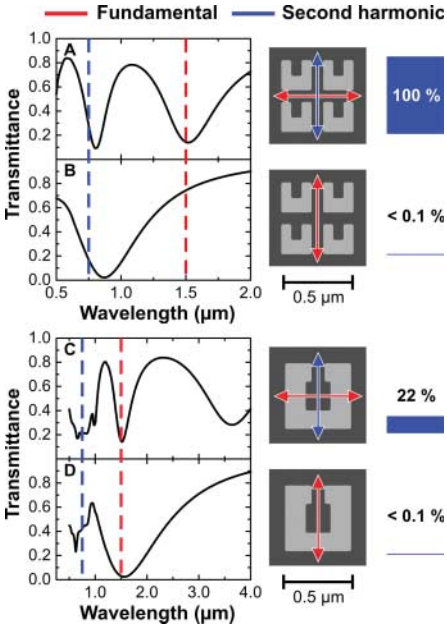

Fig. 3. Theory, presented as the experiment (see Fig. 1). The SHG source is the magnetic component of the Lorentz force on metal electrons in the SRRs.

The setup for measuring the SHG is described in the supporting online material (*22*). We expect that the SHG strongly depends on the resonance that is excited. Obviously, the incident polarization and the detuning of the laser wavelength from the resonance are of particular interest. One possibility for controlling the detuning is to change the laser wavelength for a given sample, which is difficult because of the extremely broad tuning range required. Thus, we follow an alternative route, lithographic tuning (in which the incident laser wavelength of 1.5 μm, as well as the detection system, remains fixed), and tune the resonance positions by changing the SRR size. In this manner, we can also guarantee that the optical properties of the SRR constituent materials are identical for all configurations. The blue bars in Fig. 1 summarize the measured SHG signals. For excitation of the *LC* resonance in Fig. 1A (horizontal incident polarization), we find an SHG signal that is 500 times above the noise level. As expected for SHG, this signal closely scales with the square of the incident power (Fig. 2A). The polarization of the SHG emission is nearly vertical (Fig. 2B). The small angle with respect to the vertical is due to deviations from perfect mirror symmetry of the SRRs (see electron micrographs in Fig. 1). Small detuning of the *LC* resonance toward smaller wavelength (i.e., to 1.3-μm wavelength) reduces the SHG signal strength from 100% to 20%. For excitation of the Mie resonance with vertical incident polarization in Fig. 1D, we find a small signal just above the noise level. For excitation of the Mie resonance with horizontal incident polarization in Fig. 1C, a small but significant SHG emission is found, which is again polarized nearly vertically. For completeness, Fig. 1B shows the off-resonant case for the smaller SRRs for vertical incident polarization.

Although these results are compatible with the known selection rules of surface SHG from usual nonlinear optics (*23*), these selection rules do not explain the mechanism of SHG. Following our above argumentation on the magnetic component of the Lorentz force, we numerically calculate first the linear electric and magnetic field distributions (*22*); from these fields, we compute the electron velocities and the Lorentz-force field (fig. S1). In the spirit of a metamaterial, the transverse component of the Lorentz-force field can be spatially averaged over the volume of the unit cell of size a by a by t. This procedure delivers the driving force for the transverse SHG polarization. As usual, the SHG intensity is proportional to the square modulus of the nonlinear electron displacement. Thus, the SHG strength is expected to be proportional to the square modulus of the driving force, and the SHG polarization is directed along the driving-force vector. Corresponding results are summarized in Fig. 3 in the same arrangement as Fig. 1 to allow for a direct comparison between experiment and theory. The agreement is generally good, both for linear optics and for SHG. In particular, we find a much larger SHG signal for excitation of those two resonances (Fig. 3, A and C), which are related to a finite magnetic-dipole moment (perpendicular to the SRR plane) as compared with the purely electric Mie resonance (Figs. 1D and 3D), despite the fact that its oscillator strength in the linear spectrum is comparable. The SHG polarization in the theory is strictly vertical for all resonances. Quantitative deviations between the SHG signal strengths of experiment and theory, respectively, are probably due to the simplified SRR shape assumed in our calculations and/or due to the simplicity of our modeling. A systematic microscopic theory of the nonlinear optical properties of metallic metamaterials would be highly desirable but is currently not available.

References and Notes

1. J. B. Pendry, A. J. Holden, D. J. Robbins, W. J. Stewart, *IEEE Trans. Microw. Theory Tech.* **47**, 2075 (1999).
2. J. B. Pendry, *Phys. Rev. Lett.* **85**, 3966 (2000).
3. R. A. Shelby, D. R. Smith, S. Schultz, *Science* **292**, 77 (2001).
4. T. J. Yen *et al.*, *Science* **303**, 1494 (2004).
5. S. Linden *et al.*, *Science* **306**, 1351 (2004).
6. C. Enkrich *et al.*, *Phys. Rev. Lett.* **95**, 203901 (2005).
7. A. N. Grigorenko *et al.*, *Nature* **438**, 335 (2005).
8. G. Dolling, M. Wegener, S. Linden, C. Hormann, *Opt. Express* **14**, 1842 (2006).
9. G. Dolling, C. Enkrich, M. Wegener, C. M. Soukoulis, S. Linden, *Science* **312**, 892 (2006).
10. J. B. Pendry, D. Schurig, D. R. Smith, *Science* **312**, 1780; published online 25 May 2006.
11. U. Leonhardt, *Science* **312**, 1777 (2006); published online 25 May 2006.
12. M. W. Klein, C. Enkrich, M. Wegener, C. M. Soukoulis, S. Linden, *Opt. Lett.* **31**, 1259 (2006).
13. W. J. Padilla, A. J. Taylor, C. Highstrete, M. Lee, R. D. Averitt, *Phys. Rev. Lett.* **96**, 107401 (2006).
14. D. R. Smith, S. Schultz, P. Markos, C. M. Soukoulis, *Phys. Rev. B* **65**, 195104 (2002).
15. S. O'Brien, D. McPeake, S. A. Ramakrishna, J. B. Pendry, *Phys. Rev. B* **69**, 241101 (2004).
16. J. Zhou *et al.*, *Phys. Rev. Lett.* **95**, 223902 (2005).
17. A. K. Popov, V. M. Shalaev, available at http://arxiv.org/abs/physics/0601055 (2006).
18. V. G. Veselago, *Sov. Phys. Usp.* **10**, 509 (1968).
19. M. Wegener, *Extreme Nonlinear Optics* (Springer, Berlin, 2004).
20. H. M. Barlow, *Nature* **173**, 41 (1954).
21. S.-Y. Chen, M. Maksimchuk, D. Umstadter, *Nature* **396**, 653 (1998).
22. Materials and Methods are available as supporting material on *Science* Online.
23. P. Guyot-Sionnest, W. Chen, Y. R. Shen, *Phys. Rev. B* **33**, 8254 (1986).

24. We thank the groups of S. W. Koch, J. V. Moloney, and C. M. Soukoulis for discussions. The research of M.W. is supported by the Leibniz award 2000 of the Deutsche Forschungsgemeinschaft (DFG), that of S.L. through a Helmholtz-Hochschul-Nachwuchsgruppe (VH-NG-232).

Supporting Online Material

www.sciencemag.org/cgi/content/full/313/5786/502/DC1
Materials and Methods
Figs. S1 and S2
References

26 April 2006; accepted 22 June 2006
10.1126/science.1129198

Reducing the Dimensionality of Data with Neural Networks

G. E. Hinton* and R. R. Salakhutdinov

High-dimensional data can be converted to low-dimensional codes by training a multilayer neural network with a small central layer to reconstruct high-dimensional input vectors. Gradient descent can be used for fine-tuning the weights in such "autoencoder" networks, but this works well only if the initial weights are close to a good solution. We describe an effective way of initializing the weights that allows deep autoencoder networks to learn low-dimensional codes that work much better than principal components analysis as a tool to reduce the dimensionality of data.

Dimensionality reduction facilitates the classification, visualization, communication, and storage of high-dimensional data. A simple and widely used method is principal components analysis (PCA), which finds the directions of greatest variance in the data set and represents each data point by its coordinates along each of these directions. We describe a nonlinear generalization of PCA that uses an adaptive, multilayer "encoder" network